Isospin effects in $N \approx Z$ nuclei in extended Density Functional Theory

Wojciech Satuła*
Institute of Theoretical Physics, Faculty of Physics
University of Warsaw, PL-02-093 Warsaw, Poland
Witold Nazarewicz†
Dept. of Physics and Astronomy and FRIB Laboratory
Michigan State University, East Lansing, MI 48824, USA
Institute of Theoretical Physics, Faculty of Physics
University of Warsaw, PL-02-093 Warsaw, Poland

Pacs Ref: 21.10.Hw, 21.60.Jz, 21.30.Fe, 23.40.Hc, 24.80.+y

arXiv:1510.03251v1 [nucl-th] 12 Oct 2015

Abstract

This paper overviews various phenomena related to the concept of isospin symmetry. The focus is on $N \approx Z$ nuclei, which are excellent laboratories of isospin physics. The theoretical framework applied is nuclear Density Functional Theory and its isospin- and angular-momentum projected extensions, as well as symmetry-projected multi-reference models. The topics covered include: isospin impurities, superallowed beta decays, beta-transitions in mirror nuclei, isospin breaking hadronic interactions, mirror and triplet binding energy differences, and isoscalar pairing.

1. Introduction

Isobaric spin was introduced by Heisenberg in 1932 [1] in order to explain the neutron-proton symmetry. Subsequently, the isospin symmetry has been widely used in theoretical modeling of the atomic nuclei [2, 3, 4]. Even though it is broken by the electroweak force, isospin is extremely useful for our understanding of nuclear structure and decays.

Of particular interest for isospin physics are $N \approx Z$ nuclei. Beyond ^{40}Ca, many of them are located far from the line of beta stability, in close proximity to the proton drip line. Because of the similarity of proton and neutron shell-model orbits, the $N \approx Z$ systems exhibit unique phenomena related to the attractive nature of the isoscalar component of the nuclear force. Examples are: superallowed Fermi beta decays [5], superallowed Gamow-Teller decays [6], superallowed alpha decays [7], Wigner energy [8], isoscalar pairing [9], and collective modes [10].

The atomic nuclei with enhanced sensitivity to fundamental symmetries are unique laboratories to search for signals of new physics beyond the Standard Model. The $N \approx Z$ nuclei are particularly interesting probes as the superallowed $I{=}0^+ \to I{=}0^+$ beta-decays among the isobaric analogue states in the isospin triplet allow stringent tests of the conserved vector current hypothesis and provide precise values of the strength of the weak force and the leading $V_{\rm ud}$ element of the Cabbibo-Kobayashi-Maskawa matrix. Other examples include Fermi- and Gamow-Teller ground-state beta-decays in $T{=}1/2$ mirror nuclei, which offer alternative tests of the electroweak sector. In all these cases, high-fidelity theoretical calculations of radiative corrections and isospin symmetry breaking (ISB) effects are needed to extract the crucial information from precise measurements.

The theory roadmap for this area involves ab-initio and configuration interaction (shell model) approaches, and nuclear density functional theory (DFT). The latter is the tool of choice for open-shell, deformed complex systems. The focus of this paper is on DFT-based frameworks and their extensions, including multi-reference approaches involving symmetry restoration. Such models are able to capture core-polarization effects originating from a subtle interplay between the long-range Coulomb interaction and short-range hadronic inter-nucleon forces; hence, they are particularly useful to study various aspects of electroweak interaction.

The aim of this overview is to present selected aspects of isospin physics in $N \sim Z$ nuclei in terms of theoretical approaches rooted in nuclear density functional theory. We shall start in Sec. 2 by covering the topic of isospin impurities, which reflect the degree of isospin symmetry breaking. They are responsible for isospin-forbidden rare decay modes and impact electroweak matrix elements of decays, which probe fundamental symmetries. Two examples of such decays will be discussed: the $0^+ \to 0^+$ superallowed beta-decays in Sec. 3 and Fermi- and Gamow-Teller ground-state beta-decays in $T{=}1/2$ mirror nuclei in Sec. 4. Section 5 is devoted to the mirror and triplet displacement energies sensitive to hadronic interactions, which break charge-symmetry and charge-independence. The phenomenon of proton-neutron pairing is covered in Sec. 6 in the context of a generalized DFT approach that is based on proton-neutron mixed orbitals. Finally, perspectives are given in Sec. 7.

2. Isospin impurity

The degree of isospin symmetry violation – the isospin impurity – is a result of a subtle balance between the attractive short-range strong force and the repulsive long-range Coulomb interaction that polarizes the entire nu-

*e-mail: *satula@fuw.edu.pl*
†e-mail: *witek@frib.msu.edu*

cleus. Consequently, its precise theoretical treatment requires the use of a *no-core* framework which, in heavier nuclei, is provided by nuclear DFT.

The early attempts to evaluate the degree of isospin breaking, measured in terms of the isospin impurity α_C, date back to the 1960s, see Ref. [11] for a review. These estimates, based on perturbation theory [12] or analytically solvable hydrodynamical model [13], were able to explain some gross features of α_C such as the steady increase of isospin mixing along the $N = Z$ line with increasing A or quenching of α_C with increasing $|N - Z|$. These early models, however, were not too quantitative.

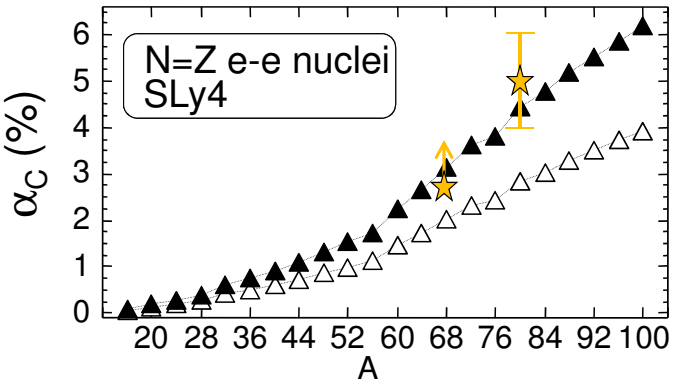

Fig. 1: Isospin impurities α_C in even-even $N = Z$ nuclei calculated with SLy4 EDF [14]. Full (open) triangles mark the AR (BR) values, respectively. Note that, the mean-field estimates (BR) are quenched by ≈30% with respect to the results of rediagonalization. Stars mark empirical values in ^{64}Ge [15] (only the lower bound is known in this case) and ^{80}Zr [16]. (Taken from Ref [17].)

The accurate calculation of the isospin impurities has been challenging. This was early realized by Engelbrecht and Lermer [18] who pointed out that the self-consistent mean-field (MF) approaches cannot be directly applied because of the spurious mixing caused by the spontaneous isospin-symmetry-breaking effects. To eliminate the problem of spurious admixtures in the wave function, we have developed a no-core MR-DFT model involving isospin projection, see also Refs. [19, 20]. The model employs self-consistent, isospin-broken MF states $|\varphi\rangle$. Self-consistency is needed to ensure that the balance between the Coulomb force and the strong interaction, represented in our model by the Skyrme energy density functional (EDF), are properly taken into account. The MF state can be formally decomposed into good-isospin basis $|T, T_z\rangle$:

$$|\varphi\rangle = \sum_{T\geq|T_z|} b_{T,T_z}|T,T_z\rangle, \qquad \sum_{T\geq|T_z|} |b_{T,T_z}|^2 = 1, \quad (1)$$

where T and $T_z = (N - Z)/2$ are the total isospin and its third component, respectively, The mixing coefficients b_{T,T_z} can be calculated using the states

$$|T,T_z\rangle = \frac{1}{\sqrt{N_{TT_z}}}\hat{P}^T_{T_zT_z}|\varphi\rangle \quad (2)$$

obtained by isospin projection after variation.

To assess the isospin mixing, one has to rediagonalize the total Hamiltonian $\hat{H}$ involving strong interaction plus the Coulomb term in the space spanned by the good-isospin basis (2):

$$|n,T_z\rangle = \sum_{T\geq|T_z|} a^n_{T,T_z}|T,T_z\rangle, \quad (3)$$

where n enumerates the eigenstates $|n, T_z\rangle$ of $\hat{H}$. The value of $n = 1$, corresponds to the isospin-mixed ground state (g.s.). The g.s. isospin-mixing parameter obtained after rediagonalization (AR) is defined as:

$$\alpha_C = 1 - |a^{n=1}_{|T_z|,T_z}|^2. \quad (4)$$

Comparison of α_C with the quantity $\alpha_C^{(\mathrm{BR})} = 1-|b_{|T_z|,T_z}|^2$ obtained before rediagonalization (BR) provides direct information about the spuriosity of MF solutions. As shown in Fig. 1, the isospin impurities exceed MF values by almost 30%.

The empirical information on isospin impurities in heavier systems is both scarce and uncertain. The values of α_C extracted from a forbidden E1 transition in ^{64}Ge [15] or from the decay of giant dipole resonance in ^{80}Zr [16] are consistent with the predictions of the isospin-projected DFT but the experimental uncertainties are too large to discriminate between different EDF parameterizations. Indeed, as shown in Fig. 2, the spread in α_C obtained with nine Skyrme EDFs, $\bar{\alpha}_C^{\mathrm{TH}} \approx 4.4\% \pm 0.3\%$, is relatively small and lies well within the experimental uncertainty limits. The figure shows the calculated impurities versus excitation energy $\Delta E_{\mathrm{T=1}}$ for the lowest $T = 1$ state in even-even $N = Z$ nuclei, which is referred to as the *doorway state*. It is seen that the larger excitation energy of the doorway state the smaller impurity, with exception of the SkO' result.

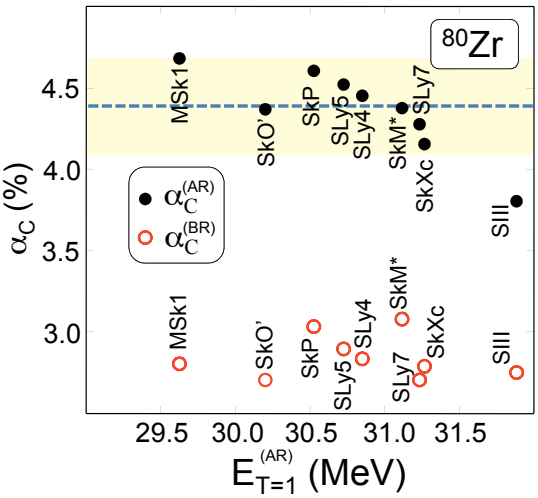

Fig. 2: Calculated isospin impurities in ^{80}Zr versus excitation energy of the doorway state. The results were obtained using the isospin projected DFT formalism with nine Skyrme EDFs. Filled (open) circles refer to AR (BR) results, respectively. The AR results lie within experimental uncertainty limits of Ref. [16] while the BR values are ruled out by the data. (Taken from Ref. [21].)

Figure 3 shows the calculated excitation energy of the doorway state for the three Skyrme EDFs: SIII [22], SLy4 [14], and SkP [23]. The self-consistent values of the

excitation energies of the doorway state are compared with the estimate $\Delta E_{\mathrm{T}=1} \approx 2\hbar\omega \approx 82/A^{1/3}$ MeV of Ref. [12] based on the perturbation theory, and with the hydrodynamical estimate $\Delta E_{\mathrm{T}=1} \approx 169A^{1/3}$ MeV of Ref. [13]. It is seen that the simple estimates of $\Delta E_{\mathrm{T}=1}$ vastly differ from the self-consistent results, both in terms of the magnitude and A-dependence. This indicates that the Coulomb mixing is a highly non-perturbative effect that requires self-consistent treatment of the interplay between short- and long-range interactions. That is why back-of-the-envelope predictions of α_C are so unreliable.

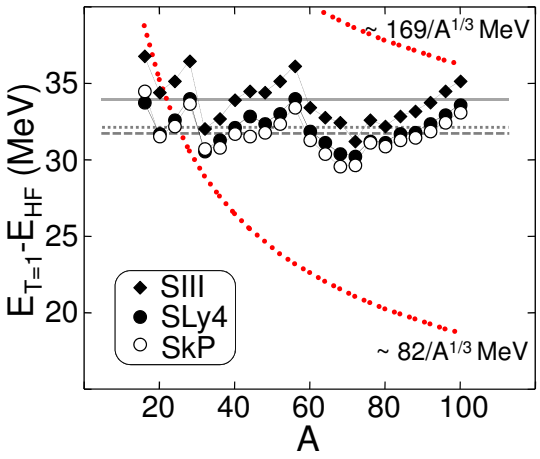

Fig. 3: Excitation energies of the doorway states $E_{\mathrm{T}=1}$ in the even-even $N{=}Z$ nuclei relative to the g.s. energies E_{HF} obtained with SIII (diamonds), SLy4 (dots), and SkP (circles) Skyrme EDFs. Horizontal lines mark the mean values. The estimates based on the perturbation theory [12] and the hydrodynamical model [13] are indicated by thick dotted lines. (Adopted from Ref. [24].)

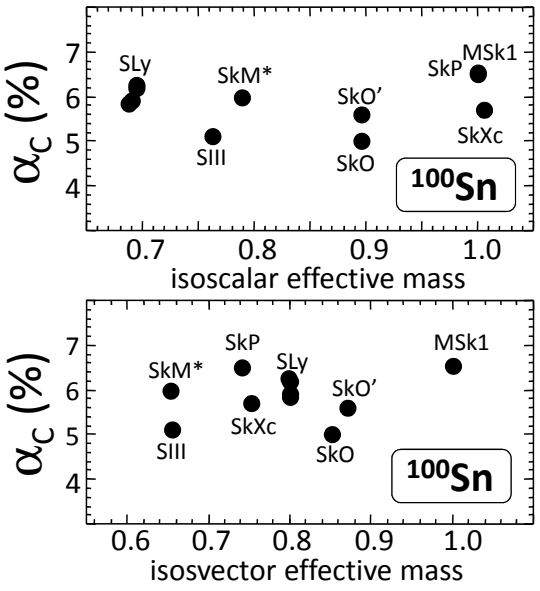

Fig. 4: Isospin impurity $\alpha_{\mathrm{C}}^{(\mathrm{AR})}$ in ^{100}Sn calculated for several Skyrme EDFs plotted as a function of the isoscalar (top) and isovector (bottom) effective mass.

Excitation energies of the doorway states and, in turn, isospin impurities, depend on EDF parameterization. It is, however, not at all obvious what EDF components are responsible for the systematic differences seen in Fig. 3. Indeed, attempts to correlate α_{C} with various bulk properties of Skyrme EDFs turned out to be fairly inconclusive. For example, no correlation has been found with the symmetry energy [21], which is the primary quantity characterizing the isovector properties of EDFs. As illustrated in Fig. 4, no clear correlation has been found between α_C and the isovector and isoscalar effective mass.

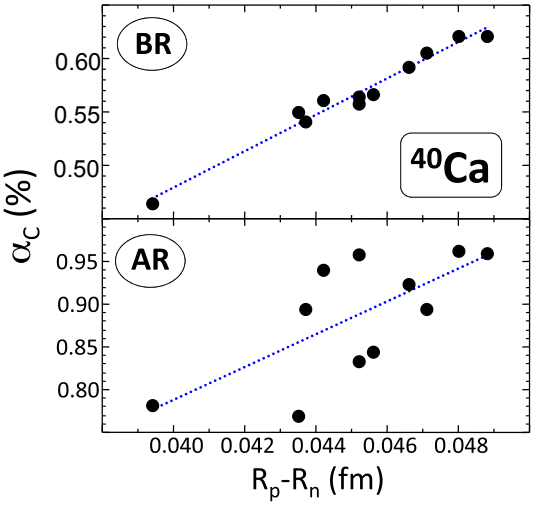

Fig. 5: Coulomb impurities in ^{40}Ca versus a difference of mean proton and neutron radii. Upper plot shows mean-field values $\alpha_{\mathrm{C}}^{(\mathrm{BR})}$. Lower plot shows true impurities $\alpha_{\mathrm{C}}^{(\mathrm{AR})}$.

We do find, however, a strong correlation between $\alpha_{\mathrm{C}}^{(\mathrm{BR})}$ and the proton skin, i.e., the difference between proton and neutron root mean square radii, see Fig. 5 and Ref. [25]. The correlation deteriorates for $\alpha_{\mathrm{C}}^{(\mathrm{AR})}$, indicating again that the isospin mixing is a non-perturbative quantity; hence difficult to estimate.

The formalism discussed above can be extended to incorporate the angular-momentum projection. In this case, the basis is created by applying the isospin ($\hat{P}^T_{T_zT_z}$) and angular-momentum ($\hat{P}^I_{MK}$) projection to $|\varphi\rangle$:

$$|I,M,K;T,T_z\rangle = \frac{1}{\sqrt{N_{TT_z;IMK}}}\hat{P}^T_{T_zT_z}\hat{P}^I_{MK}|\varphi\rangle, \qquad (5)$$

where M and K denote the magnetic quantum numbers associated with the laboratory and intrinsic z-axes, respectively [26]. Because K is not conserved, the set (5) is overcomplete. This problem can be overcome by rediagonalization of the Hamiltonian in the so-called *collective space*, spanned for each I and T by the *natural states*, $|IM;TT_z\rangle^{(i)}$ [27, 28]. The wave functions

$$|n;IM;T_z\rangle = \sum_{i,T\geq|T_z|} a^{(n)}_{iIT}|IM;TT_z\rangle^{(i)} \qquad (6)$$

obtained in the rediagonalization are labeled by the index n and conserved quantum numbers I, M, and T_z.

The double-projected and isospin-projected approaches yield very similar g.s. isospin impurities in even-even nuclei. However, there are configurations for which the model solely relying on isospin projection is insufficient.

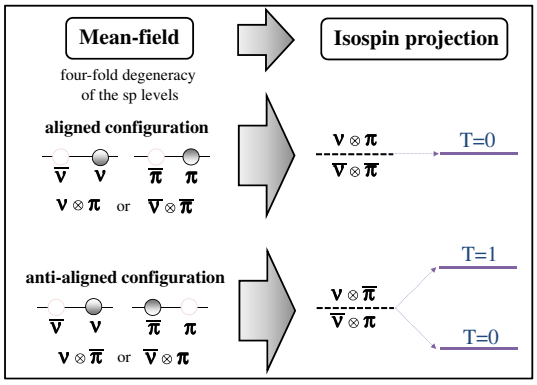

Fig. 6: Left: schematic illustration of two possible mean-field g.s. configurations in an odd-odd N=Z nucleus. Upper (lower) configuration is called aligned (anti-aligned). Right: the result of the isospin symmetry restoration. The aligned configuration is isoscalar; hence, it is insensitive to the isospin projection. The anti-aligned configuration represents a mixture of T=0 and T=1 states. The projection lifts the isospin degeneracy by lowering the T=0 level. (Taken from Ref. [29].)

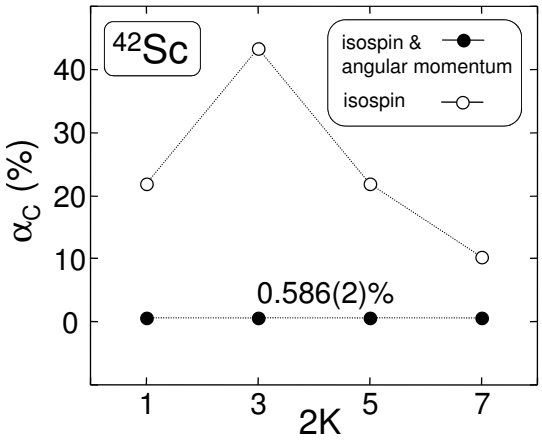

Fig. 7: Isospin impurities in ^{42}Sc, calculated for four antialigned configurations $|\nu\bar{K} \otimes \pi K\rangle$ obtained by putting the valence neutron and proton in opposite-K Nilsson orbitals originating from the $f_{7/2}$ shell. Open and full dots show the results obtained in isospin-projected and double-projected ($I = 0, T = 0$) variants, respectively. (Adopted from Ref. [30].)

Among them there are the so-called anti-aligned configurations in odd-odd $N = Z$ nuclei, which are crucial for calculations of ISB corrections to the superallowed beta-decay involving the $T = 1, J = 0^+$ states in odd-odd nuclei. These states are not representable by a single MF configuration as shown schematically in Fig. 6. Indeed, the odd proton and odd neutron can form either the aligned or anti-aligned configuration. The aligned configuration represents an isoscalar $T = 0, J \neq 0$ state. The anti-aligned configuration, however, manifestly breaks the isospin symmetry being an equal mixture of isoscalar and isovector states. The calculations indicate [29] that the T=0 and T=1 components projected from the anti-aligned configuration strongly mix through the Coulomb interaction leading to unphysically large isospin impurities. Double-projected approach is free from such pathologies. This is demonstrated in the lower part of Fig. 7 for a representative case of ^{42}Sc.

It can be shown [24] that the isospin projection technique can be safely used within nuclear DFT. Augmenting the isospin projection with the angular-momentum projection leads to a number of theoretical issues. Not only the numerical complexity of computations increases but also the uncontrolled singularities appear in the energy kernels [30]; this essentially eliminates a possibility to use modern EDFs with density-dependent terms [31]. To overcome this problem, regularization schemes have been proposed [32, 33] but they are difficult in practical implementations. Until a workable solution is developed, a practical option is to use Hamiltonian-based EDFs, such as the SV force [22] augmented by the tensor terms, or the recently developed SLyMR forces that include three- and four-body terms [34].

All the existing parameterizations of the density-independent Skyrme EDF are characterized by a nonstandard saturation mechanism driven by a very low isoscalar effective mass $\frac{m^*}{m} \approx 0.4$. The low effective mass affects the overall performance of those forces, impairing such key properties as the symmetry energy, level density, and level ordering. The low value of $\frac{m^*}{m}$ also impacts the isospin mixing. In particular, in the case of ^{80}Zr discussed above, the SV EDF yields $\alpha_{\rm C} \approx 2.8\%$, which is considerably smaller than the mean value, $\bar{\alpha}_{\rm C} \approx 4.4 \pm 0.3\%$, obtained by averaging over the EDFs shown in Fig. 2. The lack of a reasonable Hamiltonian-based Skyrme EDF is probably the most critical deficiency of the current self-consistent approach. Nonetheless, one has to admit that the EDFs with low effective masses perform surprisingly well when used in the context of no-core-configuration-interaction (NCCI) extensions [35, 36, 37, 38]

3. Isospin-symmetry-breaking corrections to the superallowed $J^\pi = 0^+, T = 1 \to J^\pi = 0^+, T = 1$ beta decays

The superallowed $J^\pi = 0^+, T = 1 \to J^\pi = 0^+, T = 1$ beta transitions are of particular importance for testing various aspects of the electro-weak sector of the Standard Model. What makes these pure Fermi decays so useful is the conserved vector current (CVC) hypothesis, which states that the vector current is not renormalized in the nuclear medium. This implies that the product of the statistical rate function f and partial half-life t for the superallowed $I = 0^+, T = 1 \to I = 0^+, T = 1$ Fermi beta-decay should be nucleus-independent and equal to:

$$ft = \frac{K}{G_{\rm V}^2 |M_{\rm F}^{(\pm)}|^2} = \text{const}\,, \qquad (7)$$

where $K/(\hbar c)^6 = 2\pi^3 \hbar \ln 2/(m_{\rm e}c^2)^5 = 8120.2787(11) \times 10^{-10}\,\text{GeV}^{-4}\text{s}$ is a universal constant; $G_{\rm V}$ stands for the vector coupling constant for semi-leptonic weak interaction; and $M_{\rm F}^{(\pm)}$ is the nuclear matrix element of the isospin operator $\hat{T}_\pm$.

In reality, the relation (7) holds only approximately and must be slightly amended to account for radiative processes and isospin-symmetry breaking effects. Fortunately, the radiative and ISB corrections are small, of the order

of a few percent, and this allows us to express the rate conveniently as:

$$\mathcal{F}t \equiv ft(1+\delta'_{\rm R})(1+\delta_{\rm NS}-\delta_{\rm C}) = \frac{K}{2G_{\rm V}^2(1+\Delta_{\rm R}^{\rm V})}, \quad (8)$$

with the left-hand side being nucleus independent. In Eq. (8), $\Delta_{\rm R}^{\rm V} = 2.361(38)\%$ stands for the nucleus-independent part of the radiative correction [39], $\delta'_{\rm R}$ is a transition-dependent (Z-dependent) but nuclear-structure-independent part of the radiative correction [39, 40], and $\delta_{\rm NS}$ denotes the nuclear-structure-dependent part of the radiative correction [41, 40]. The ISB correction $\delta_{\rm C}$ is a many-body correction to the nuclear matrix element:

$$|M_{\rm F}^{(\pm)}|^2 = 2(1-\delta_{\rm C}), \quad (9)$$

accounting for the isospin-symmetry violation in the atomic nuclei, see Refs. [42, 43, 44, 45, 5] and references cited therein.

In spite of explicit dependence on theoretical input and the related uncertainties in the calculated radiative and ISB corrections, the superallowed beta-decays provide today's most accurate value of the vector coupling constant $G_{\rm V}$. Moreover, they enable a very accurate verification of the CVC hypothesis and provide precise information on the leading matrix element $V_{\rm ud} = G_{\rm V}/G_\mu$ of the CKM three-generation quark mixing matrix [46, 47, 44, 45, 48, 5]. This is so because the leptonic coupling constant, $G_\mu/(\hbar c)^3 = 1.16637(1)\times 10^{-5}$ GeV^{-2}, is well known from the muon decay [48]. The uncertainty of $V_{\rm ud}$ extracted from the superallowed beta-decays is almost by an order of magnitude smaller as compared to the values obtained from neutron or pion decays [48].

In search for physics beyond the Standard Model, precision is of utmost importance. Only those transitions that have ft-values measured with an accuracy $\leq 0.3\%$ are acceptable. The *canonical* set of transitions used over the last decade to test the Standard Model consists of 13 such cases spreading over a wide range of masses from A=10 (^{10}Ca) to A=74 (^{74}Rb), see [44, 45, 5]. With the CVC hypothesis confirmed, it is possible to extract $V_{\rm ud}$ by averaging over several transitions. This feature makes the superallowed beta-decay strategy very attractive. Recently, the canonical set has been extended by a measurement of the beta-decay of ^{38}Ca [49, 50]. Moreover, the superallowed decay of ^{18}Ne is within experimental reach [51].

The ISB corrections $\delta_{\rm C}$ were computed in diverse nuclear models, see Refs. [52, 45, 53, 54, 55, 56, 57]. The standard in this field has been set by Hardy and Towner (HT) [40, 43, 44, 45, 5] who have used the nuclear shell model to account for the configuration mixing effect in conjunction with the mean-field potential needed to account for a radial mismatch of proton and neutron single-particle (s.p.) wave functions due to the long-range Coulomb polarization [53]. Such a description has certain practical advantages. For instance, it allows for an independent fine-tuning of various model's ingredients. But it also leads to internal inconsistencies. In particular, the HT model violates the SU(2) commutation rules for the bare isospin operators as pointed out in Refs. [58, 59]. Unfortunately, the associated uncertainty is difficult to quantify.

The self-consistent multi-reference DFT involving the isospin- and angular-momentum projections [25, 24, 57, 29] is an interesting alternative to the fine-tuned phenomenological HT approach. This is a *no-core* theory, which is capable of treating rigorously the rotational symmetry and explicit breaking of isospin symmetry. The correct balance between the Coulomb and hadronic forces is maintained by self-consistency requirements. The approach allows for a rigorous treatment of the Fermi matrix elements using bare isospin operators. The recently proposed NCCI extensions of the framework [36, 37, 60] allow to take into account more correlations due to inclusion of (multi)particle-(multi)hole configurations. As already mentioned, the weakest point of the formalism is the lack of a reasonable Hamiltonian-based Skyrme EDF. One should stress, however, that δ_C does not depend on the absolute magnitude of isospin mixing but rather on a difference between parent and daughter states [56], i.e., it is a less sensitive quantity.

The MR-DFT calculations of $\delta_{\rm C}$ involving single reference states in parent and daughter nuclei are carried out as follows. The superallowed $0^+ \to 0^+$ Fermi beta-decay proceeds between the g.s. $|I=0, T\approx 1, T_z=\pm 1\rangle$ of the even-even nucleus and its isospin-analogue partner $|I=0, T\approx 1, T_z=0\rangle$ in the $N=Z$ odd-odd nucleus. The corresponding transition matrix element is:

$$M_{\rm F}^{(\pm)} = \langle I=0, T\approx 1, T_z=\pm 1|\hat{T}_\pm|I=0, T\approx 1, T_z=0\rangle. \quad (10)$$

Within the MR-DFT, the parent g.s. is approximated by a projected state

$$|I=0, T\approx 1, T_z=\pm 1\rangle = \sum_{T\geq 1} c_T^{(\psi)} \hat{P}^T_{\pm 1,\pm 1} \hat{P}^{I=0}_{0,0} |\psi\rangle, \quad (11)$$

where $|\psi\rangle$ is the g.s. of the even-even nucleus obtained in the self-consistent Hartree-Fock calculations. The state $|\psi\rangle$ is unambiguously defined by filling in the pairwise doubly-degenerate levels of protons and neutrons up to the Fermi level. The daughter state is approximated by

$$|I=0, T\approx 1, T_z=0\rangle = \sum_{T\geq 0} c_T^{(\varphi)} \hat{P}^T_{0,0} \hat{P}^{I=0}_{0,0} |\varphi\rangle, \quad (12)$$

where the self-consistent Slater determinant $|\varphi\rangle \equiv |\bar{\nu}\otimes\pi\rangle$ (or $|\nu\otimes\bar{\pi}\rangle$) represents the anti-aligned configuration, selected by placing the odd neutron and the odd proton in the lowest available time-reversed (or signature-reversed) s.p. orbits. The isospin-projected state shown in Fig. 6, based on the $|\varphi\rangle$ configuration that manifestly breaks the isospin symmetry, is indeed a preferred way to access the $|T\approx 1, I=0\rangle$ states in odd-odd $N=Z$ nuclei.

The anti-aligned configurations in odd-odd $N=Z$ nuclei are not uniquely defined. In the signature-symmetry-restricted calculations, there are in general three anti-aligned Slater determinants with the s.p. angular momenta (alignments) of the valence protons and neutrons pointing along the Ox, Oy, or Oz axes of the intrinsic shape defined by means of the long (Oz), intermediate (Ox), and short (Oy) principal axes of the nuclear mass distribution, respectively. Thus far, in spite of persistent efforts, no self-consistent tilted-axis g.s. solutions have been found. Various properties of these linearly dependent solutions, hereafter referred to as $|\varphi_{\rm X}\rangle$, $|\varphi_{\rm Y}\rangle$, and $|\varphi_{\rm Z}\rangle$, are discussed in detail in Ref. [29] and will not be repeated here.

In a MR-DFT double-projection approach based on a single reference state, the only way to deal with the shape-current orientation ambiguity is to calculate three independent beta-decay matrix elements corresponding to each orientation and average over the resulting values of $\delta_{\rm C}$. Such an strategy was adopted in Ref. [29], which contains the calculated corrections for the canonical set of superallowed transition as well as predictions for yet-unmeasured cases. The calculated corrections are in reasonable agreement with the HT results as shown in Fig. 8. Both sets of corrections systematically overestimate the RPA results of Ref. [55].

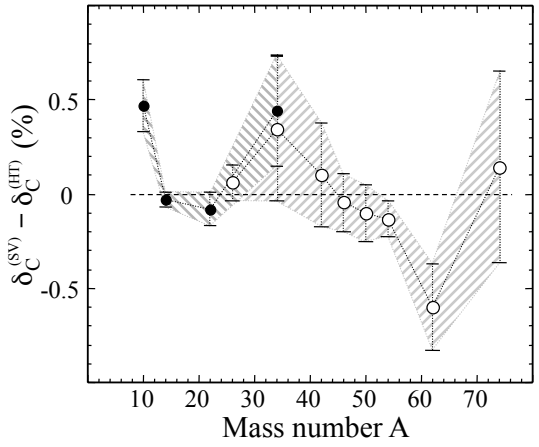

Fig. 8: Differences between the ISB corrections to 12 precisely measured superallowed $0^+ \to 0^+$ decays (excluding A=38) calculated in Refs. [29] (SV) and [40] (HT). Shaded band shows the combined SV+HT error. (Taken from Ref. [29].)

With the set of ISB corrections obtained in Ref. [29], one obtains $\overline{\mathcal{F}t} = 3073.6(12)\,$s, which gives $|V_{\rm ud}| = 0.97397(27)$. This value is in excellent agreement with the HT result [40], $|V_{\rm ud}^{\rm (HT)}| = 0.97418(26)$, and the central value obtained from the neutron decay, $|V_{\rm ud}^{(\nu)}| = 0.9746(19)$ [61]. Taking the calculated $|V_{\rm ud}|$ and combining it with $|V_{\rm us}| = 0.2252(9)$ and $|V_{\rm ub}| = 0.00389(44)$ from the 2010 Particle Data Group [61], one obtains

$$|V_{\rm ud}|^2 + |V_{\rm us}|^2 + |V_{\rm ub}|^2 = 0.99935(67), \qquad (13)$$

which implies that the unitarity of the first row of the CKM matrix is satisfied with a precision better than 0.1%. A survey of the $|V_{\rm ud}|$ values obtained using different methods is shown in Fig. 9.

The solutions $|\varphi_{\rm X}\rangle$, $|\varphi_{\rm Y}\rangle$, and $|\varphi_{\rm Z}\rangle$, differ by at most a few hundred keV in energy. Hence, there is no obvious preference for a choice of reference state. Moreover, the orientation-dependent effects originate, predominantly, from the time-odd fields of the nuclear MF. Hence, the orientation effects are present only in odd-odd nucleus adding up to a difference between parent and daughter nuclei. The averaging procedure applied in Ref. [29] should be considered as a purely practical solution. The shape-current-orientation ambiguity has motivated us to extend the formalism to allow for a dynamical mixing of states that are projected from low-lying (multi)particle-(multi)hole self-consistent MF configurations. In the context of the $\delta_{\rm C}$ calculations, the idea is to mix 0^+ states

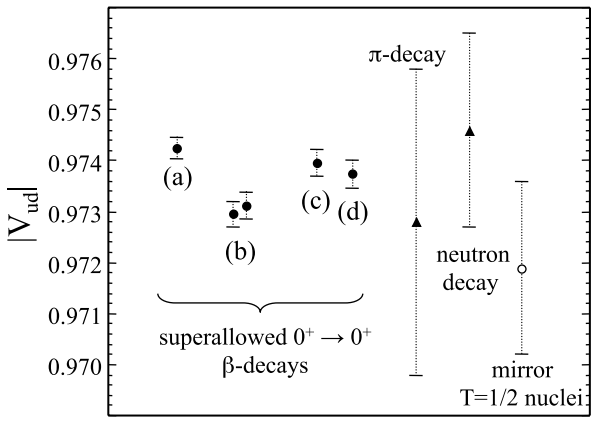

Fig. 9: A survey of the $|V_{\rm ud}|$ values obtained using different methods: (a) Ref. [40]; (b) Ref. [55]; (c) Ref. [29] with SV; (d) Ref. [29] with SHZ2. The values obtained form pion-decay [62], neutron-decay [61], and beta-decays in T=1/2 mirror nuclei [63] are shown for comparison. (Taken from Ref. [29].)

projected from $|\varphi_{\rm X}\rangle$, $|\varphi_{\rm Y}\rangle$, and $|\varphi_{\rm Z}\rangle$ configurations, respectively. In such an approach, the I=0 wave functions in an odd-odd N=Z nucleus are approximated by:

$$|n;\, I=0, T_z=0\rangle = \sum_{i={\rm X,Y,Z}} \sum_{T'\geq 0} f_{iT'}^{(n;\, I=0, T_z=0)} \hat{P}_{0,0}^{T'} \hat{P}_{0,0}^{I=0} |\varphi_i\rangle, \qquad (14)$$

where the coefficients $f_{iT'}^{(n;\, I=0,T_z=0)}$ are obtained by solving the Hill-Wheeler-Griffin (HWG) equation, and n enumerates the HWG eigenstates. The HWG equation has, typically, three linearly independent solutions which, instead of n, can be conveniently labeled by approximate isospin quantum number: $|I=0, T\approx 0, T_z=0\rangle$, $|I=0, T\approx 1, T_z=0\rangle$, and $|I=0, T\approx 2, T_z=0\rangle$.

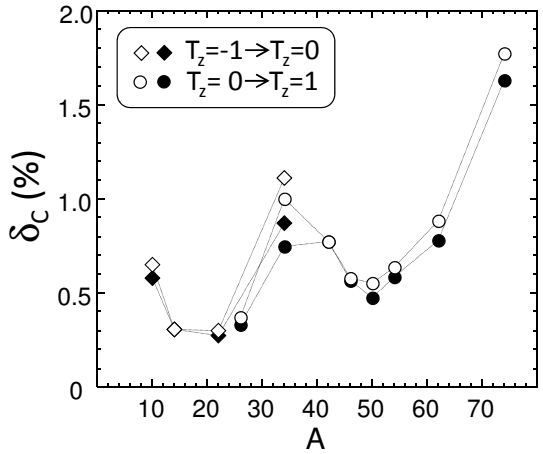

Fig. 10: Comparison of the ISB corrections to the 12 canonical superallowed $0^+ \to 0^+$ transitions calculated in Ref. [29] (open symbols) and in Ref. [60] (filled symbols). In the latter calculations, the 0^+ states projected from $|\varphi_{\rm X}\rangle$, $|\varphi_{\rm Y}\rangle$, and $|\varphi_{\rm Z}\rangle$ configurations were mixed dynamically by solving the HWG equation. In the former, matrix elements were calculated independently for each orientation and averaged afterwards.

The new set of the ISB corrections calculated using this prescription is displayed in Fig. 10; the detailed values

can be found in Ref. [60]. The improved corrections are somewhat smaller that the values of Ref. [29] obtained by averaging over orientations. This difference, however, has almost no influence on $\overline{\mathcal{F}t}$ and $|V_{\rm ud}|$. Indeed the new values $\overline{\mathcal{F}t} = 3073.7(11)$s and $|V_{\rm ud}| = 0.97396(25)$, calculated with the updated set of experimental ft values taken from Ref. [45], almost perfectly match the previous numbers [29].

Towner and Hardy [43] proposed a confidence level (CL) test to check a consistency of the calculated ISB corrections. The underlying assumptions are: (*i*) validity of the CVC hypothesis up to at least $\pm 0.03\%$ and (*ii*) validity of the calculated nuclear-structure-dependent corrections $\delta_{\rm NS}$ [41]. These two assumptions allow to calculate *empirical* corrections:

$$\delta_{\rm C}^{\rm (exp)} = 1 + \delta_{\rm NS} - \frac{\overline{\mathcal{F}t}}{ft(1+\delta'_{\rm R})}. \qquad (15)$$

By treating the value of $\overline{\mathcal{F}t}$ as an adjustable parameter, one can bring $\delta_{\rm C}^{\rm (exp)}$ as close as possible to the calculated $\delta_{\rm C}$ by minimizing the appropriate χ^2. With the new set of corrections calculated in Ref. [60], the χ^2 per degree of freedom (n_d=11) drops from χ^2/n_d=10.2 [29] to 6.3. This number is still much larger than the values reported in Ref. [43], which are: 1.7 for the Damgård model [52], 0.4 for the shell-model with Woods-Saxon wave functions [45], 2.3 for the shell-model with Hartree-Fock wave functions [45], and 2.1 for the relativistic DFT+RPA model of Ref. [55]. The main contribution to the χ^2-value in our model can be associated with the sudden increase in $\delta_{\rm C}$ due to a single ^{62}Ga$\rightarrow^{62}$Zn transition, which contributes more than 62% to the total χ^2 budget.

4. Ground-state beta-transitions in T=1/2 mirror nuclei

The T=1/2 mirror nuclei offer an alternative way to test the CVC hypothesis [63]. These nuclei decay via the mixed Fermi and Gamow-Teller (GT) transitions. Hence, apart from the radiative and the ISB corrections, the values of $G_{\rm F}$ and $V_{\rm ud}$ also depend on the ratio of statistical rate functions $f_{\rm A}/f_{\rm V}$ for the axial-vector and vector interactions, and the ratio $\rho \approx \lambda M_{\rm GT}/M_{\rm F}$ of nuclear matrix elements, where $\lambda = g_{\rm A}/g_{\rm V}$ denotes the ratio of axial-vector and vector coupling constants.

The CVC hypothesis implies that the vector coupling constant is $g_{\rm V} = 1$. The axial-vector current is partially conserved; this implies that the axial-vector coupling constant gets renormalized in the nuclear medium. The effective axial-vector coupling constant, $g_A^{\rm (eff)} = q_s g_{\rm A}$, is quenched by an A-dependent factor q_s with respect to the free neutron decay value $g_{\rm A} \approx -1.2701(25)$. Quenching factors deduced from comparison of large-scale nuclear shell model (NSM) calculations with experiment are: $q_s \approx 0.82$, 0.77 [64], and 0.74 [65] in the *p*-, *sd*-, and *pf*-shell region, respectively. In the region $A \approx 130$, a large value of $q_s \approx 0.57$ has been extracted [66], see however [67]. To account for the mass dependence of q_s in shell-model calculations, a phenomenological expression

$$q_s = 1 - 0.19\left(\frac{A}{16}\right)^{0.35} \qquad (16)$$

has been proposed [64] for $A \leq 40$.

The origin of the quenching is not fully understood. It is usually related to missing correlations in the wave function; truncation of model space; and – in the context of *ab initio* models – two-body currents [68, 69, 70]. Much work in this area has been done in relation to the double-beta decay [71, 70, 72] and WIMP scattering [73]. Recent study of the Ikeda sum rule in β^- decays of ^{14}C and ^{22,24}O performed in Ref. [74] estimate quenching due to the two-body currents to be $q_s = 0.84 - 0.92$. This range is consistent with experimental data on ^{90}Zr [75, 76].

Recently, a systematic study of both the GT and Fermi ground-state transitions in the T=1/2 mirror *sd*- and *pf*-shell T=1/2 mirror nuclei with $17 \leq A \leq 55$ have been carried out using the self-consistent NCCI approach [77]. Within the NCCI model the wave function reads [cf. Eq. (6)]:

$$\begin{aligned} |n;\, IM;\, T_z\rangle &= \sum_{i,j} a_{ij}^{(n;IM;T_z)} |\varphi_j;\, IM;T_z\rangle^{(i)} \qquad (17)\\ &= \sum_{i,j} \sum_{K,T\geq|T_z|} f_{ijKT}^{(n;IM;T_z)} \hat{P}^T_{T_zT_z} \hat{P}^I_{MK} |\varphi_j\rangle\,. \end{aligned}$$

When compared to the isospin- and angular-momentum MR-DFT wave-function (6), the NCCI wave function contains additional summation over the configurations (Slater determinants) $|\varphi_j\rangle$. In the present implementation of the formalism, we use the same Skyrme interaction to compute the configurations $|\varphi_j\rangle$ and to mix the isospin- and angular-momentum-projected states $|\varphi_j;\, IM;T_z\rangle^{(i)}$.

The model was tested for the ^{6}He$\rightarrow^6$Li GT beta decay. Matrix element for this transition, $|M_{\rm GT}|$=2.1645(43), is precisely known from the recent measurement [78]. Figure 11 shows a difference between the calculated and experimental GT matrix element as a function of the NCCI configuration space considered. The first point corresponds to the case of no configuration mixing. Here, the wave functions $|0^+_{\rm gs}\rangle$ and $|1^+_{\rm gs}\rangle$ are projected from the optimal (energy-wise) Slater determinants. Next, keeping the parent wave function $|0^+_{\rm gs}\rangle$ fixed, we enrich the configuration space of the daughter nucleus by admixing the 1^+ states projected from the lowest particle-hole (ph) and the two lowest ($2ph$) particle-hole configurations: $|1^+_{\rm gs}\rangle \rightarrow |1^+_{\rm ph}\rangle \rightarrow |1^+_{\rm 2ph}\rangle$. This causes an increase of the matrix element circa 3% above the experimental value. The extension of the configuration space of ^{6}He by admixing excited 0^+ states hardly impacts this result, see Fig. 11. This test indicates that NCCI is capable of capturing the main features of the wave functions that are important for a reliable reproduction of the GT matrix element. Unfortunately, the model underbinds ^{6}Li and overbinds ^{6}He; hence we have not great confidence in its accuracy for this specific GT transition. This is, however, not surprising as the current DFT approaches and their MR-DFT and NCCI extensions have not been optimized to experimental data in light nuclei.

Theoretical ground-state GT matrix elements in the T=1/2 mirror *sd*- and *pf*-shell nuclei ranging from A=17 till 55 are shown in Fig. 12. The NCCI results with the SV$_{\rm SO}$ EDF were obtained using the HFODD solver [27, 79] that has been augmented with the NCCI module. The details of calculations follow Ref. [77]. It is seen that

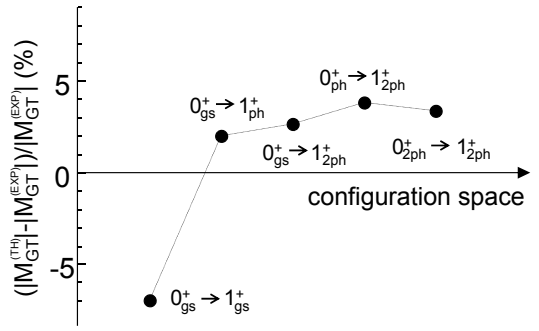

Fig. 11: GT ^{6}He$\rightarrow^6$Li matrix element computed in NCCI relative to experiment [78] as a function of NCCI configuration space.

the NCCI results are fairly close to shell model predictions [80, 65, 81]. The consistency between these two theoretical approaches is visualized in Fig. 12 (bottom), which shows that both models correlate well with experimental data. As discussed in Ref. [77], this similarity is quite surprising since the models differ in many aspects.

The model-independent Ikeda sum rule [82] serves as an important indicator of the quality of theoretical models of GT decay. In the A=39, T=1/2 nuclei, which can be viewed as one-hole systems, inclusion of all possible *ph* excitations within the *sd*-shell space exhausts 99% of the sum rule [77]. Recently, we have performed similar calculations for the A=23, T=1/2 systems, which are complex, open-shell deformed nuclei. The calculations, involving eight deformed particle-hole configurations, were performed using two variants of the NCCI model: the full model involving the isospin- and angular-momentum projection and its simplified variant involving only the angular-momentum projection. The results are shown in Fig. 13. As anticipated, both methods give almost identical matrix elements for the GS transition. This is because the effect of isospin mixing in the ground states of nuclei considered is very small. Note however, that the variant involving the angular-momentum projection only captures mere 40% of the Ikeda sum rule. At the same time, the full variant of the model accounts for the 85% of the sum rule. The example shows that the proper treatment of isospin in excited states is critical for the sum rule evaluation.

The full variant of the model involving double-projection is necessary to compute the ISB corrections to the Fermi branch of beta-decay in the T=1/2 mirror nuclei. These nuclei offer the independent way to verify the CVC hypothesis and to study the CKM matrix [63, 84]. A set of the ISB corrections calculated with the MR-DFT technique was published in Ref. [57], and the NCCI results can be found in Table 1 of Ref. [77]. The NCCI predictions are shown in Fig. 14 and compared to the SM results of Ref. [83]. It is seen that the NCCI corrections, although slightly smaller on average, are fairly consistent with SM. Figure 15 shows a difference between these two sets of calculations. The shaded area marks the error band calculated as $\sqrt{(\Delta\delta_C^{(NCCI)})^2 + (\Delta\delta_C^{(SM)})^2}$ under the assumption of 10% error on the NCCI results due to a basis cut-off.

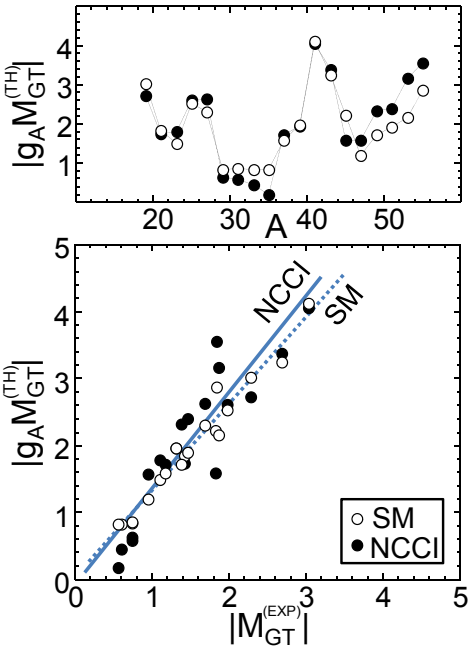

Fig. 12: Top: ground-state GT matrix elements in T=1/2 medium-mass mirror nuclei calculated using NCCI (filled circles) [77] and shell-model (SM) approaches (open circles) [80, 65, 81]. Bottom: a correlation between the theoretical and experimental matrix elements. Solid (dashed) line represents a linear fit to the NCCI (SM) results.

5. Mirror and Triplet binding energy differences, and the Nolen-Schiffer anomaly

Strong interaction is, predominantly, invariant with respect to rotations in the isospin space. This fact is rather well established experimentally and confirmed theoretically. Indeed, most nuclear many-body approaches, including shell-model and DFT models, use interactions that are scalar in the isospace. The Skyrme interaction is a prime example of an isospin invariant effective force that has long been used to compute various nuclear properties.

On the other hand, there also exists a firm experimental evidence that the strong interaction contains small isospin-breaking components. For example, the nucleon-nucleon (NN) scattering data reveal small differences in phase shifts and scattering lengths. In the $^1S_0$ channel, the scattering lengths for neutron-neutron (nn), neutron-proton (np), and proton-proton (pp) scattering are: $a_{nn} \approx -18.9$ fm, $a_{np} \approx -23.7$ fm, and $a_{pp} \approx -17.3$ fm, respectively [85]. A detailed analysis of scattering data, in particular phase shifts and scattering lengths, shows that the nn interaction is 1% stronger than pp interaction and that the np interaction is 2.5% stronger than the average of nn and pp interactions [85]. (These figures include corrections for electromagnetic effects and refer solely to the strong nucleon-nucleon interaction.) On the fundamental level, the isospin symmetry is broken due to different masses and electromagnetic interactions of u and d quarks [86].

Albeit small, isospin violation considerably influences global properties of finite nuclei such as binding energies. It is well known that models including isospin-invariant strong force and the Coulomb interaction alone have dif-

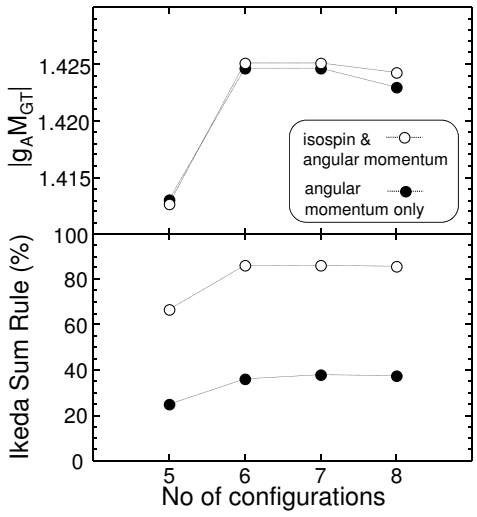

Fig. 13: Top: GT matrix element for the g.s.→g.s. transition ^{23}Mg→^{23}Na versus the number of particle-hole configurations taken in the NCCI calculation involving angular-momentum projection (dots) and isospin- and angular-momentum projection (circles). Bottom: the predicted Ikeda sum rule for the g.s. configuration of ^{23}Mg.

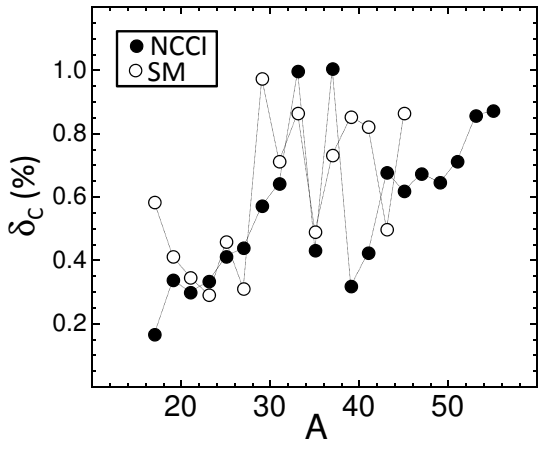

Fig. 14: ISB corrections to the ground-state Fermi transitions in T=1/2 mirror nuclei obtained in NCCI [77] (dots) and the SM+Woods-Saxon model of Ref. [83] (circles).

ficulties in reproducing the Mirror Displacement Energies (MDEs), the differences of binding energies of mirror nuclei (Nolen-Schiffer anomaly [87]):

$$\mathrm{MDE} = BE\left(T, T_z = -T\right) - BE\left(T =, T_z = +T\right). \quad (18)$$

These models has also problems in reproducing the Triplet Displacement Energies (TDEs). The TED indicator is defined as:

$$\mathrm{TDE} = BE\left(T = 1, T_z = -1\right) + BE\left(T = 1, T_z = +1\right) - 2BE\left(T = 1, T_z = 0\right), \quad (19)$$

and is a measure of the binding-energy curvature within the isospin triplet [36, 88, 89, 90].

It is customary to classify components of the nuclear force in terms of the SU(2) symmetry of isospace. Here, one defines charge independence as invariance under rotation in the isospin space. The charge symmetry, on the other hand, can be defined as an invariance under a rotation by 180° about the y isospin axis. Violation of this symmetry is referred to as charge symmetry breaking (CSB).

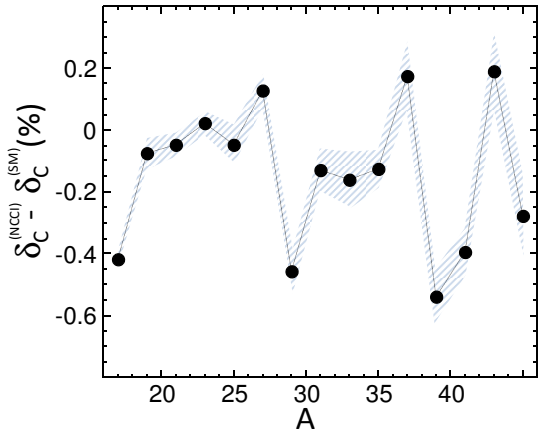

Fig. 15: Difference between ISB corrections to the g.s. Fermi decays in T=1/2 mirror nuclei calculated with NCCI [77] and the SM+Woods-Saxon model of Ref. [83]. The shaded area marks the theoretical uncertainty.

In the language of NN force, CSB implies a difference between *pp* and *nn* interactions in the same channel, $V_{nn} \neq V_{pp}$. Moreover, if in the isospin-triplet $T = 1$ channel $V_{np} \neq (V_{nn} + V_{pp})/2$ the force is charge-independence-breaking (CIB). The data on NN scattering lengths indicate that the strong NN interaction must contain both the CSB and CIB strong components. On the fundamental level, the CSB mostly originates from the difference in masses of the proton and neutron which affects the kinetic energies and influences the boson exchange. The CIB originates mostly from the pion mass splitting, see Refs. [85, 91]. In nuclear medium, the CSB and CIB components of the effective strong force are accessible through the MDEs and TDEs, respectively.

A detailed classification of various components of the strong NN force was proposed by Henley and Miller [92, 91]. They divided different components of the strong force into four classes. According to this classification, the isospin invariant (i.e., isoscalar) NN interactions are called the class I forces. They commute with the total nuclear isospin operator, $\left[V_{\mathrm{I}}^{(\mathrm{NN})}, \mathbf{T}_A\right] = 0$. The class II isotensor forces maintain charge symmetry, but break charge independence as $\left[V_{\mathrm{II}}^{(\mathrm{NN})}, \mathbf{T}_A\right] \neq 0$. The class III isovector forces break both the charge independence and charge symmetry, but are symmetric under interchange of nucleonic indices in the isospace. Such forces distinguish between the *nn* and *pp* systems and vanish in the *np* system. Forces of class II and class III do not mix isospin *only* at the two-body level; hence they contribute to the isospin mixing in finite nuclei. Isovector forces of class IV break both symmetries and mix isospin already at the two-body level. Those forces do not influence the *nn* and *pp* systems, but induce a spin-dependent isospin mixing effects in the *np* system.

The isospin symmetry breaking components of NN interactions were studied in *ab inito* approaches [85, 93]. Hadronic ISB terms of *effective* NN interactions were in-

vestigated in the context of nuclear shell model [94, 95, 96, 97, 98, 99, 88, 100] and mean-field approaches [101, 54, 102, 103]. A note of caution is in order here. First, any attempt to extract effective NN interactions from spectroscopic data should first account for the coupling to the many-body continuum [104, 105] in the presence of isospin-conserving nuclear forces. If neglected, or not treated carefully, the continuum effects can alter the results of such analyses [106, 107, 108]. Second, in-medium nuclear effective interactions (G-matrix) contain contributions from the Coulomb force. If the Coulombic contributions are not treated precisely during the renormalization procedure, they can result in the presence of CSB and CIB components, which can then be incorrectly labelled as "hadronic".

To investigate the effect of hadronic CSB and CIB terms and their possible influence on isospin mixing and ISB corrections, one can apply the local Skyrme-DFT approach. To this end, one needs to generalize the formalism to the case of *pn*-mixed quasiparticle states [109]. Such an extension leads to isospin-invariant EDFs that depend explicitly on local *pn* densities and currents. Recently, this formalism was applied to the Hartree-Fock case by admitting *pn* mixing in the particle-hole channel [110, 111]. Within this framework, the explicit ISB comes entirely from the electrostatic interaction.

In the next step, the *pn*-mixed formalism can be extended to accommodate the CSB and CIB hadronic components. The *pn*-mixing is a necessary prerequisite that allows to study these terms in a fully self-consistent manner. Since the discrepancies between the experimental and theoretical MDEs and TDEs are small [103, 36] they can be modelled in terms of class II (CIB) and class III (CSB) zero-range corrections to the conventional Skyrme force:

$$\hat{V}_{\rm II}(i,j) = \frac{1}{2}t_0^{\rm II}\,\delta\left(\mathbf{r}_{ij}\right)\left(3\hat{\tau}_3(i)\hat{\tau}_3(j) - \vec{\tau}(i)\circ\vec{\tau}(j)\right), \quad (20)$$

$$\hat{V}_{\rm III}(i,j) = \frac{1}{2}t_0^{\rm III}\,\delta\left(\mathbf{r}_{ij}\right)\left(\hat{\tau}_3(i) + \hat{\tau}_3(j)\right), \quad (21)$$

where $t_0^{\rm II}$ and $t_0^{\rm III}$ are the ISB force parameters that are adjusted to reproduce empirical TDEs and MDEs. The spin-exchange has been omitted as it leads to a trivial rescaling of the parameters. The associated ISB contributions to the EDF are:

$$\begin{aligned}\mathcal{H}_{\rm II} &= \frac{1}{2}t_0^{\rm II}\left(\rho_n^2 + \rho_p^2 - 2\rho_n\rho_p - 2\rho_{np}\rho_{pn}\right.\\ &\quad\left. -\boldsymbol{s}_n^2 - \boldsymbol{s}_p^2 + 2\boldsymbol{s}_n\cdot\boldsymbol{s}_p + 2\boldsymbol{s}_{np}\cdot\boldsymbol{s}_{pn}\right), \quad (22)\\ \mathcal{H}_{\rm III} &= \frac{1}{2}t_0^{\rm III}\left(\rho_n^2 - \rho_p^2 - \boldsymbol{s}_n^2 + \boldsymbol{s}_p^2\right). \quad (23)\end{aligned}$$

Note, that class II forces depend on the *pn*-mixed particle ρ_{np} and spin $\boldsymbol{s}_{np}$ densities, respectively. Hence, these forces can be included only within the *pn*-mixed DFT formalism. The class III forces, on the other hand, depend only on the standard *pp* and *nn* densities and can be, therefore, treated within the conventional Skyrme-DFT approach.

In order to control the total isospin of the nucleus in the *pn*-mixing calculations, we use a three-dimensional isocranking approach [112]. This technique is analogous to the well known cranking method in real space, which is commonly used in high-spin physics. It is realized by adding the isocranking term to the mean-field Hamiltonian $\hat{h}$,

$$\hat{h}' = \hat{h} - \vec{\lambda}\circ\vec{t} = \hat{h} - \lambda_1\hat{t}_1 - \lambda_2\hat{t}_2 - \lambda_3\hat{t}_3, \quad (24)$$

where $\vec{t} = \frac{1}{2}\vec{\tau}$ stands the s.p. isospin operator and $\vec{\lambda}$ is the isocranking frequency. By adjusting the frequencies $\vec{\lambda}$, one can control both the length and direction of the isospin vector. In practical applications, $\vec{\lambda}$ is parameterized as follows:

$$\vec{\lambda} = (\lambda'\sin\theta'\cos\phi, \lambda'\sin\theta'\sin\phi, \lambda'\cos\theta' + \lambda_{\rm off}). \quad (25)$$

The offset $\lambda_{\rm off} \neq 0$ is introduced to facilitate calculations with the Coulomb interaction [110, 111]. By choosing the offset properly, one can compensate for the effect of the electrostatic interaction on the third component of the isocranking term. In this way, $\lambda_{\rm off}$ helps to avoid s.p. level crossings while tilting the isocranking axis and, consequently, keeps the expectation value of the total isospin fixed [113].

In order to study the influence of the ISB forces on nuclear binding energies, we have performed the isocranking calculations for the A=34 isospin triplet. In these test calculations, the Coulomb interaction has been switched off. The results with the CIB force (20) are shown in Fig. 16. As anticipated, this force impacts the binding energy of

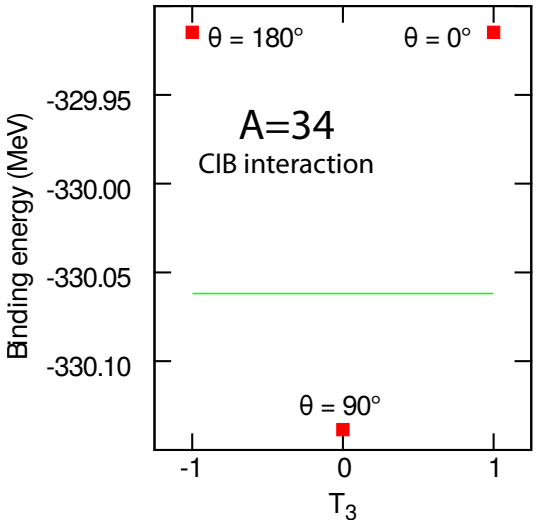

Fig. 16: Binding energy for the A=34 isospin triplet calculated using the isocranking approach with the isoscalar SV Skyrme force without Coulomb, augmented by the CIB (class II) interaction (20) with $t_0^{\rm II}$=20 MeV.

$T_z = 0$ system without affecting the binding energies of $T_z = \pm 1$ triplet members. Hence, it changes the TDE indicator without affecting MDE. On the other hand, as shown in Fig. 17, the class III force (21) changes MDEs without affecting TDEs. This implies that the simplest strategy it to adjust the coupling constants $t_0^{\rm II}$ and $t_0^{\rm III}$ to TDEs and MDEs, respectively.

Figures 18 and 19 show preliminary results of the calculated MDEs and TDEs in the isospin triplets ranging from A=22 to 55. The calculations have been done using the SV Skyrme EDF with Coulomb, augmented by the CIB

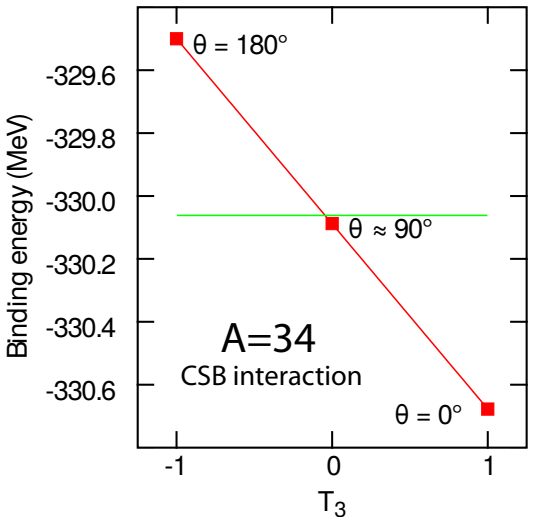

Fig. 17: Similar as in Fig. 16 but for the CSB (class III) interaction (21) with $t_0^{\rm III} = -8\,$MeV.

and CSB forces with $t_0^{\rm II} = 20\,$MeV and $t_0^{\rm III} = -8\,$MeV, respectively. It is seen that a generalized *pn*-mixed Skyrme DFT approach is able to reproduce experimental data on TEDs and MEDs.

The *pn*-mixed ISB DFT formalism can address the evolution of ISB effects with angular momentum in rotational bands of $T = \frac{1}{2}$ and $T = 1$ nuclei. Such effects has been investigated within shell-model framework [95, 96, 114, 98, 99, 88, 115]. The quantities of interest are mirror energy differences (MEDs) and triplet energy differences (TEDs), similar to MDEs and TDEs but defined through excitation energies ΔE_I of rotational states at a given angular momentum I:

$$\begin{aligned} \mathrm{MED}(I) = \Delta E_I \left(T = \frac{1}{2}, T_z = -\frac{1}{2}\right) \\ -\Delta E_I \left(T = \frac{1}{2}, T_z = +\frac{1}{2}\right), \end{aligned} \tag{26}$$

$$\begin{aligned} \mathrm{TED}(I) = \Delta E_I \left(T = 1, T_z = -1\right) \\ -2\Delta E_I \left(T = 1, T_z = 0\right) \\ +\Delta E \left(T = 1, T_z = +1\right). \end{aligned} \tag{27}$$

In general, while shell-model studies indicate that the ISB hadronic forces are as important as the Coulomb interaction for the explanation of angular momentum dependence of MEDs and TEDs, the overall picture is not fully understood, especially in the upper *fp* shell.

One of the key features of the NCCI model based on Skyrme forces with low effective mass is its ability to reproduce rotational bands. The preliminary calculations performed for ^{48}Cr, a key nucleus in the *f*-shell concerning collective properties, indicate that our model is capable of reproducing its collective g.s. band fairly well [116]. This opens an opportunity to address MED and TED effects in a non-perturbative way, as a function of angular momentum, incorporating the ISB effects self-consistently along the rotational path.

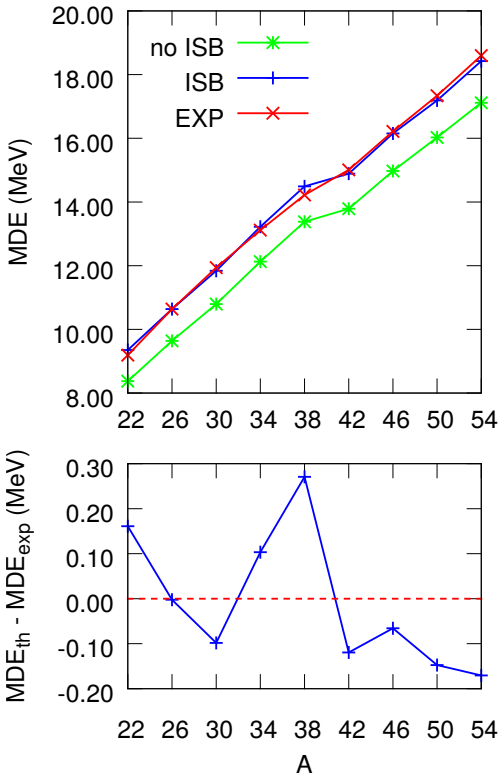

Fig. 18: Top: experimental and calculated (with and without hadronic ISB terms) MDEs in the isospin triplets ranging from A=22 to 55. Bottom: MDE residuals pertaining to ISB calculations.

6. Proton-neutron pairing

Superfluidity and superconductivity belong to the most spectacular examples of emergent phenomena in many-body systems. They appear at different physical scales and in different environments in atomic, condensed matter, nuclear, and elementary particle physics. The BCS mechanism [117] behind the pair condensate works irrespective of details of the underlying interaction that couples fermions into the Cooper pairs at the Fermi surface. In low-energy nuclear physics, nucleonic pairing affects many properties of finite nuclei and nucleonic matter [118, 119].

Nucleonic Cooper pairs can exist in many flavors. In terms of isospin quantum number, one can talk about isovector triplet ($T = 1$) and isovector singlet ($T = 0$) pairs. The conventional *nn* and *pp* pairing has isovector character, while the *pn* pairing can be either isovector or isoscalar. The first attempts to incorporate the *pn*-pairing into the independent quasi-particle approach date back to the mid-sixties [120, 121, 122]. These models were further developed into a consistent formalism allowing for simultaneous treatment of isovector and isoscalar pairs [123, 124, 125, 126, 127]. The formalism was further extended to include stretched T=0 pairs ($\alpha\alpha$ *pn*-pairing) in Ref. [128]. These early approaches encountered difficulties in predicting coexisting $T = 0$ and $T = 1$ pairing-phases. The solutions of the early models based on separable seniority-type interactions could be conveniently classified in terms of a single parame-

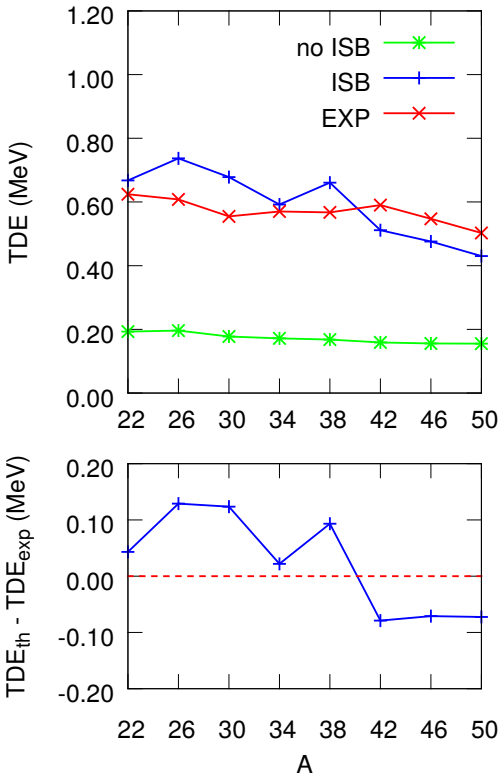

Fig. 19: Similar to Fig. 18 but for TDEs.

ter, the value of isoscalar-to-isovector matrix element ratio $x \equiv G^{T=0}/G^{T=1}$. In particular, for $N = Z$ nuclei, the solution is of a pure isovector type for $x < 1$; for $x = 1$ the isovector and isoscalar phases are degenerate; and for $x > 1$ there appears a pure isoscalar solution. These models were later extended [129] to include particle-number projected wave functions. For $x > x_{\rm crit} \approx 1.1$, the extended models have produced coexistence of $T = 0$ and $T = 1$ phases. It was also predicted that for $x \geq 1.3$ the isoscalar pairing component could be the source of the Wigner energy [129, 8]. Following these developments, various models have been proposed to look for signatures of the isoscalar pairing phase and explain the Wigner energy [130, 131, 132, 133, 134, 135, 9, 136].

In spite of many efforts, however, a comprehensive theory of nucleonic pairing still eludes us. This negatively impacts our understanding of nuclei in the vicinity of the $N = Z$ line, where the *pn*-correlations are expected to be strongest. Indeed, a consistent approach to the the *pn*-pairing problem requires implementing the *pn*-mixing on the mean-field level, whereby the s.p. wave functions are combinations of proton and neutron components. Basic self-consistency principles require such a mixing to accompany any hypothetical *pn*-mixing in the pairing channel. Moreover, the stability and existence of the *pn*-pairing condensate may critically depend on the restoring force related to the *pn*-mixing on the mean field level, and thus both must be simultaneously included in the theoretical description. As discussed above, the DFT frameworks incorporating the *pn*-mixing have been developed recently [110, 111]. This constitutes the first step towards building a consistent symmetry-unrestricted superfluid DFT approach with the complete *pn*-mixing. The experience gathered so far indicates that in order to capture structure of $N \approx Z$ nuclei, the *pn*-mixed formalism should be further extended to include the restoration of number symmetry and proper treatment of isospin [113, 24].

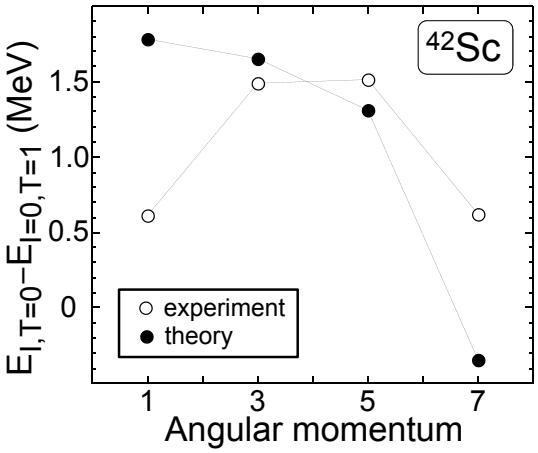

Fig. 20: Experimental (circles) and calculated (NCCI; dots) excitation energies of the $T = 0$ states in ^{42}Sc relative to the 0^+ ground state.

A need for the enhancement of the deuteron-like $J = 1^+, T = 0$ pairing channel is apparent in the present Skyrme-NCCI approach, which accounts relatively well for low-spin states but has systematic problems with the $J = 1, T = 0$ matrix elements in $N = Z$ nuclei. This is illustrated in Fig. 20 showing the calculated and experimental $T = 0$ multiplet in ^{42}Sc. It is seen that the antialigned state $J = 1^+, T = 0$ is strongly underbound and the stretched $I = 7^+$ level is overbound. A similar situation has been encountered in ^{6}Li where the NCCI model strongly underbinds $J = 1, T = 0$ matrix elements [60].

7. Prospects

In this paper, we overview selected topics related to isobaric spin in $N \sim Z$ nuclei. We demonstrate that "no-core" and self-consistency aspects of nuclear DFT are essential for our quantitative understanding of isospin breaking. The approximate nature of isospin poses many theoretical challenges as the underlying symmetry is broken both explicitly and spontaneously, and the isospin mixing is highly non-perturbative due to a mismatch between the ranges of electrostatic and strong forces. To handle this situation theoretically, one needs to go beyond the usual single-reference DFT formalism. The proposed multi-reference DFT framework, based on isospin- and angular-momentum projected wave functions, provides a very satisfactory description of isospin breaking effects in beta decay.

The future developments will undoubtedly utilize the newly developed isospin-invariant density functional framework [110, 111]. The *pn*-mixed DFT formalism needs to be extended to the particle-particle channel by including pairing interaction of both isoscalar and isovector types. This will enable us to study the importance of the isoscalar pairing densities and fields on the structure of $N \approx Z$ nuclei and the impact of *pn*-mixing on single- and

double-beta decays. It seems, however, that in order to capture key structural aspects of $N = Z$ nuclei, the *pn*-mixed formalism should be further extended to include the restoration of particle number, isospin, and angular momentum. This will require an appropriate NCCI extension.

In quantitative calculations, quality input is crucial. A construction and optimization of a realistic Hamiltonian-based EDF is among the most urgent needs. This development will not only improve the predictive power of the model but will also help addressing the burning question pertaining to the role of ISB interaction components.

Acknowledgement

Useful discussions with Jacek Dobaczewski are gratefully acknowledged. Paweł Bączyk is thanked for providing material presented in Sec. 5 prior to publication [116]. This article is based upon work supported by the Polish National Science Centre (NCN) under Contract No. 2012/07/B/ST2/03907 and by the U.S. Department of Energy, Office of Science, Office of Nuclear Physics under Award Numbers No. DOE-DE-SC0013365 (Michigan State University) and No. de-sc0008511 (NUCLEI SciDAC Collaboration). The CSC−IT Center for Science Ltd, Finland, is acknowledged for the allocation of computational resources.

References

[1] W. Heisenberg, Z. Phys. **77**, 1 (1932).

[2] E.P. Wigner, Phys. Rev. **51**, 106 (1937).

[3] D. Robson, Annu. Rev. Nucl. Sci. **16**, 119 (1966).

[4] D.H. Wilkinson, ed. *Isospin in nuclear physics*, (North Holland, Amsterdam, 1969).

[5] J.C. Hardy and I.S. Towner, Phys. Rev. C **91**, 025501 (2015).

[6] C.B. Hinke *et al.*, Nature **486**, 341 (2012).

[7] S.N. Liddick *et al.*, Phys. Rev. Lett. **97**, 082501 (2006).

[8] W. Satuła, D.J. Dean, J. Gary, S. Mizutori, and W. Nazarewicz, Phys. Lett. **407B**, 103 (1997).

[9] S. Frauendorf and A.O. Macchiavelli, Prog. Part. Nucl. Phys. **78**, 24-90 (2013).

[10] T. Nakatsukasa, K. Matsuyanagi, I. Hamamoto, and W. Nazarewicz, Nucl. Phys. **A573**, 333 (1994).

[11] N. Auerbach, Phys. Rep. **98**, 273 (1983).

[12] L.A. Sliv and Yu.I. Kharitonov, Phys. Lett. **16**, 176 (1965).

[13] A. Bohr, J. Damgård, and B. Mottelson, in *Nuclear Structure*, ed. by A. Hossian *et al.* (North-Holland Publ. Co., Amsterdam, 1967).

[14] E. Chabanat, *et al.*, Nucl. Phys. **A627** (1997) 710; **A635** (1998) 231.

[15] E. Farnea *et al.*, Phys. Lett. **B551**, 56 (2003).

[16] A. Corsi *et al.*, Acta Phys. Pol. **B42**, 619 (2011); Phys. Rev. C **84**, 041304 (2011).

[17] W. Satuła, J. Dobaczewski, M. Konieczka, and W. Nazarewicz, arXiv:1307:1550.

[18] C.A. Engelbrecht and R.H. Lemmer, Phys. Rev. Lett. **24**, 607 (1970).

[19] E. Caurier, A. Poves, and A. Zucker, Phys. Lett. B **96**, 11 (1980); **96**, 15 (1980).

[20] E. Caurier and A. Poves, Nucl. Phys. **A385**, 407 (1982).

[21] W. Satuła, J. Dobaczewski, W. Nazarewicz, and M. Rafalski, Acta Phys. Polon. B **42**, 415 (2011).

[22] M. Beiner, H. Flocard, N. Van Giai, and P. Quentin, Nucl. Phys. **A238**, 29 (1975).

[23] J. Dobaczewski, H. Flocard, and J. Treiner, Nucl. Phys. A **422**, 103 (1984).

[24] W. Satuła, J. Dobaczewski, W. Nazarewicz, and M. Rafalski, Phys. Rev. C **81**, 054310 (2010).

[25] W. Satuła, J. Dobaczewski, W. Nazarewicz, and M. Rafalski, Phys. Rev. Lett. **103**, 012502 (2009).

[26] P. Ring and P. Schuck, *The Nuclear Many-Body Problem* (Springer-Verlag, Berlin, 1980).

[27] J. Dobaczewski, W. Satuła, B.G. Carlsson, J. Engel, P. Olbratowski, P. Powałowski, M. Sadziak, J. Sarich, N. Schunck, A. Staszczak, M.V. Stoitsov, M. Zalewski, and H. Zduńczuk, Comput. Phys. Commun. **180**, 2361 (2009).

[28] H. Zduńczuk, W. Satuła, J. Dobaczewski, and M. Kosmulski, Phys. Rev. C **76**, 044304 (2007).

[29] W. Satuła, J. Dobaczewski, W. Nazarewicz, and T.R. Werner, Phys. Rev. C **86**, 054316 (2012).

[30] W. Satuła, J. Dobaczewski, W. Nazarewicz, M. Borucki, and M. Rafalski, Int. J. Mod. Phys. **E20**, 244 (2011).

[31] M. Bender, P.-H. Heenen, and P.-G. Reinhard, Rev. Mod. Phys. **75**, 121 (2003).

[32] D. Lacroix, T. Duguet, and M. Bender, Phys. Rev. C **79**, 044318 (2009).

[33] W. Satuła and J. Dobaczewski, Phys. Rev. C **90**, 054303 (2014).

[34] J. Sadoudi, M. Bender, K. Bennaceur, D. Davesne, R. Jodon, and T. Duguet, Phys. Scr. **T154**, 014013 (2013).

[35] B. Bally, B. Avez, M. Bender, and P.-H. Heenen, Phys. Rev. Lett. **113**, 162501 (2014).

[36] W. Satuła, J. Dobaczewski, M. Konieczka, and W. Nazarewicz, Acta Phys. Polonica B**45**, 167 (2014).

[37] W. Satuła, J. Dobaczewski, and M. Konieczka, JPS Conf. Proc. **6**, 020015 (2015).

[38] W. Nazarewicz, P.-G. Reinhardt, W. Satuła, and D. Vretenar, Eur. Phys. J. A **50**, 20 (2014).

[39] W.J. Marciano and A. Sirlin, Phys. Rev. Lett. **96**, 032002 (2006).

[40] I.S. Towner and J.C. Hardy, Phys. Rev. C **77**, 025501 (2008).

[41] I.S. Towner, Phys. Lett. **B333**, 13 (1994).

[42] J.C. Hardy and I.S. Towner, Phys. Rev. C **79**, 055502 (2009).

[43] I.S. Towner and J.C. Hardy, Phys. Rev. C **82**, 065501 (2010).

[44] I.S. Towner and J.C. Hardy, Rep. Prog. Phys. **73**, 046301 (2010).

[45] J.C. Hardy and I.S. Towner, J. Phys. G: Nucl. Part. Phys. **41**, 114004 (2014).

[46] N. Cabibbo, Phys. Rev. Lett. **10**, 531 (1963).

[47] M. Kobayashi and T. Maskawa, Prog. Theor. Phys. **49**, 652 (1973).

[48] K.A. Olive *et al.* (Particle Data Group), Chin. Phys. C **38**, 090001 (2014).

[49] H.I. Park, J.C. Hardy, V.E. Iacob, M. Bencomo, L. Chen, V. Horvat, N. Nica, B. T. Roeder, E. Simmons, R.E. Tribble, and I. S. Towner, Phys. Rev. Lett. **112**, 102502 (2014).

[50] B. Blank *et al.*, Eur. Phys. J. A **51**, 8 (2014).

[51] A.T. Laffoley *et al.*, Phys. Rev. C **92**, 025502 (2015).

[52] J. Damgård, Nucl. Phys. A**130**, 233, (1969).

[53] W.E. Ormand and B.A. Brown, Phys. Rev. C **52**, 2455 (1995).

[54] H. Sagawa, N. Van Gai, and T. Suzuki, Phys. Rev. C **53**, 2163 (1996).

[55] H. Liang, N. Van Giai, and J. Meng, Phys. Rev. C **79**, 064316 (2009).

[56] N. Auerbach, Phys. Rev. C **78**, 035502 (2009).

[57] W. Satuła, J. Dobaczewski, W. Nazarewicz, and M. Rafalski, Phys. Rev. Lett. **106**, 132502 (2011).

[58] G.A. Miller and A. Schwenk, Phys. Rev. C **78**, 035501 (2008).

[59] G.A. Miller and A. Schwenk, Phys. Rev. C **80**, 064319 (2009).

[60] W. Satuła, J. Dobaczewski, and M. Konieczka, in preparation.

[61] K. Nakamura *et al.* (Particle Data Group), J. Phys. G **37**, 075021 (2010).

[62] D. Pocanic *et al.*, Phys. Rev. Lett. **93**, 181803 (2004).

[63] O. Naviliat-Cuncic and N. Severijns, Phys. Rev. Lett. **102**, 142302 (2009).

[64] W.-T. Chou, E.K. Warburton, and B.A. Brown, Phys. Rev. C **47**, 163 (1993).

[65] G. Martinez-Pinedo, A. Poves, E. Caurier, and A.P. Zucker, Phys. Rev. C **53**, R2602 (1996).

[66] E. Caurier, F. Nowacki, and A. Poves, Phys. Lett. B **711**, 62 (2012).

[67] M. Horoi and B. A. Brown, Phys. Rev. Lett. **110**, 222502 (2013).

[68] S. Vaintraub, N. Barnea, and D. Gazit, Phys. Rev. C **79**, 065501 (2009).

[69] J. Menéndez, D. Gazit, and A. Schwenk, Phys. Rev. Lett. **107**, 062501 (2011).

[70] J. Engel, F. Šimkovic, and P. Vogel, Phys. Rev. C **89**, 064308 (2014).

[71] J.D. Holt and J. Engel, Phys. Rev. C **87**, 064315 (2013).

[72] J.M. Yao, L.S. Song, K. Hagino, P. Ring, and J. Meng, Phys. Rev. C **91**, 024316 (2015).

[73] P. Klos, J. Menéndez, D. Gazit, and A. Schwenk, Phys. Rev. D **88**, 083516 (2013).

[74] A. Ekström, G.R. Jansen, K.A. Wendt, G. Hagen, T. Papenbrock, S. Bacca, B. Carlsson, and D. Gazit, Phys. Rev. Lett. **113**, 262504 (2014).

[75] K. Yako *et al.*, Phys. Lett. **B615**, 193 (2005).

[76] M. Sasano *et al.*, Phys. Rev. C **79**, 024602 (2009).

[77] M. Konieczka, P. Bączyk, and W. Satuła, arXiv:1509.0448.

[78] A. Knecht *et al.*, Phys. Rev. Lett. **108**, 122502 (2012).

[79] N. Schunck, J. Dobaczewski, J. McDonnell, W. Satuła, J.A. Sheikh, A. Staszczak, M. Stoitsov, and P. Toivanen, Comput. Phys. Commun. **183**, 166 (2012).

[80] B.A. Brown and B.H. Wildenthal, At. Data Nucl. Data Tables **33**, 347 (1985).

[81] T. Sekine, J. Cerny, R. Kirchner, O. Klepper, V.T. Koslowsky, A. Płochocki, E. Roeckl, D. Schardt, and B. Sherrill, Nucl. Phys. **A467** (1987) 93.

[82] K. Ikeda, Prog. Theor. Phys. **31**, 434 (1964).

[83] N. Severijns, M. Tandecki, T. Phalet, and I.S. Towner, Phys. Rev. C **78**, 055501 (2008).

[84] O. Naviliat-Cuncic and N. Severijns, Eur. Phys. J. A **42**, 327 (2009).

[85] R. Machleidt, Phys. Rev. C **63**, 024001 (2001).

[86] Sz. Borsanyi, S. Durr, Z. Fodor, C. Hoelbling, S.D. Katz, S. Krieg, L. Lellouch, T. Lippert, A. Portelli, K.K Szabo, and B.C. Toth, Science **347**, 1452 (2015).

[87] J.A. Nolen and J.P. Schiffer, Ann. Rev. Nuc. Sci. **19**, 471 (1969).

[88] K. Kaneko, Y. Sun, T. Mizusaki, and S. Tazaki, Phys. Rev. C **89**, 031302(R) (2014).

[89] X.L. Tu, Y. Sun, Y.H. Zhang, H.S. Xu, K. Kaneko, Yu.A. Litvinov, and M. Wang, J. Phys. G **41**, 025104 (2014).

[90] M.A. Bentley, S.M. Lenzi, S.A. Simpson, and C. Aa. Diget, Phys. Rev. C**92**, 024310 (2015).

[91] G.A. Miller, and W.H.T. van Oers, *Symmetries and Fundamental Interactions in Nuclei* edited by W.C. Haxton and E.M. Henley (World Scientific, Singapore, 1995).

[92] E.M. Henley, and G.A. Miller, in *Mesons in Nuclei*, edited by M. Rho and D.H. Wilkinson (North Holland, Amsterdam, 1979), p. 405.

[93] R.B. Wiringa, S. Pastore, S.C. Pieper, and G.A. Miller, Phys. Rev. C **88**, 044333 (2013).

[94] W.E. Ormand and B.A. Brown, Nucl. Phys. A**491**, 1 (1989.

[95] A.P. Zuker, S.M. Lenzi, G. Martinez-Pinedo, and A. Poves, Phys. Rev. Lett. **89**, 142502 (2002).

[96] M.A. Bentley and S.M. Lenzi, Prog. Part. Nucl. Phys. **59**, 497 (2007).

[97] C. Qi and F.R. Xu, Nucl. Phys. A**814**, 48 (2008).

[98] K. Kaneko, T. Mizusaki, Y. Sun, S. Tazaki, and G. de Angelis, Phys. Rev. Lett. **109**, 092504 (2012).

[99] K. Kaneko, Y. Sun, T. Mizusaki, and S. Tazaki, Phys. Rev. Lett. **110**, 172505 (2013).

[100] Yi Hua Lam, N.A. Smirnova, and E. Caurier, Phys. Rev. C **87**, 054304 (2013).

[101] H. Sagawa, N. Van Giai, and T. Suzuki, Phys. Lett. B**353**, 7 (1995).

[102] B.A. Brown, Phys. Rev. C **58**, 220 (1998).

[103] B.A. Brown, W.A. Richter, and R. Lindsay, Phys. Lett. **B483**, 49 (2000).

[104] R.G. Thomas, Phys. Rev. **88**, 1109 (1952).

[105] J.B. Ehrman, Phys. Rev. **81**, 412 (1951).

[106] L.V. Grigorenko, I.G. Mukha, I.J. Thompson, and M.V. Zhukov, Phys. Rev. Lett. **88**, 042502 (2002).

[107] N. Michel, W. Nazarewicz, and M. Płoszajczak, Phys. Rev. C **82**, 044315 (2010).

[108] C. Yuan, C. Qi, F. Xu, T. Suzuki, and T. Otsuka, Phys. Rev. C **89**, 044327 (2014).

[109] E. Perlińska, S.G. Rohoziński, J. Dobaczewski, and W. Nazarewicz, Phys. Rev. C **69**, 014316 (2004).

[110] K. Sato, J. Dobaczewski, T. Nakatsukasa, and W. Satuła, Phys. Rev. C **88**, 061301(R) (2013).

[111] J.A. Sheikh, N. Hinohara, J. Dobaczewski, T. Nakatsukasa, W. Nazarewicz, and K. Sato, Phys. Rev. C **89**, 054317 (2014).

[112] S. Głowacz, W. Satuła, and R.A. Wyss, Eur. Phys. J. **A19** (2004) 33.

[113] W. Satuła and R. Wyss. Phys. Rev. Lett. **86**, 4488 (2001); **87**, 052504 (2001).

[114] P.J. Davies *et al.*, Phys. Rev. Lett. **111**, 072501 (2013).

[115] J. Henderson *et al.*, Phys. Rev. C **90**, 051303 (2014).

[116] P. Bączyk, M. Konieczka, and W. Satuła, in preparation.

[117] J. Bardeen, L.N. Cooper, and J.R. Schrieffer, Phys. Rev. **108**, 1175 (1957).

[118] A. Bohr, B.R. Mottelson, and D. Pines, Phys. Rev. **110**, 936, (1958).

[119] R.A. Broglia and V. Zelevinsky, editors *Fifty Years of Nuclear BCS*, World Scientific, (2012).

[120] A. Goswami, Nucl. Phys. **60**, 228 (1964).

[121] A. Goswami and L.S. Kisslinger, Phys. Rev. **140**, B26 (1965).

[122] P. Camiz, A. Covello, and M. Jean, Nouvo Cimento **36**, 663 (1965); **42**, 199 (1966).

[123] H.T. Chen, G.L. Struble, and A. Goswami, Nucl. Phys. **88**, 208 (1966).

[124] H.T. Chen and A. Goswami, Nucl. Phys. **88**, 208 (1966).

[125] H.T. Chen and A. Goswami, Phys. Lett. **B24**, 257 (1967).

[126] A.L. Goodman, G.L Struble, and A. Goswami, Phys. Lett. **B26**, 260 (1968).

[127] A.L. Goodman, G.L Struble, J. Bar-Touv, and A. Goswami, Phys. Rev. **C2**, 380 (1970).

[128] A.L. Goodman, Nucl. Phys. **A186**, 475 (1972).

[129] W. Satuła and R. Wyss, Phys. Lett. **B393**, 1 (1997).

[130] K. Neergard, Phys. Rev. C**80**, 044313 (2009).

[131] N. Sandulescu, D. Negrea, and C.W. Johnson, Phys. Rev. C **86**, 041302(R) (2012).

[132] I. Bentley and S. Frauendorf, Phys. Rev. C **88**, 014322 (2013).

[133] B.G. Carlsson and J. Toivanen, Phys. Rev. C **89**, 054324 (2014).

[134] D. Negrea and N. Sandulescu, Phys. Rev. C **90**, 024322 (2014).

[135] I. Bentley, K. Neergard, and S. Frauendorf, Phys. Rev. C **89**, 034302 (2014).

[136] M. Sambarto, N. Sandulescu, and C.W. Johnson, Phys. Lett. **B740**, 137 (2015).